Monte Carlo Simulation of the Low-Voltage Arc Mode in Plasma Diodes*

S. N. SALINGER† AND J. E. ROWE

Electron Physics Laboratory, Department of Electrical Engineering, The University of Michigan, Ann Arbor, Michigan

(Received 30 March 1967; in final form 8 March 1968)

A statistical simulation of the low-voltage arc mode of plasma diodes is carried out on a large-scale digital computer to ascertain the importance of various thermalization and transport mechanisms. The computer experiment is two-dimensional and utilizes Monte Carlo techniques to study the low-voltage arc in neon at $p=2$ Torr, current $=4$ A, and diode spacing $=2.37$ cm. Results on the potential distribution, electron-density distribution, and electron-energy density function are presented and discussed. The theoretical results are correlated with experimental results.

I. INTRODUCTION

The development of plasma-diode thermionic converters operating in the low-voltage arc, or ignited, mode has indicated the need for a complete theoretical understanding of this type of discharge. The system analyzed here is a hot-cathode plasma diode with parallel-plane electrode geometry operating in the low-voltage arc mode. Although the electrode spacing is considerably greater than that characteristic of thermionic converters, the basic technique can be applied to close-spaced cesium thermionic diodes. Despite the extensive previous work, many aspects of the behavior of this mode have not yet been resolved. Extensive reviews of the previous studies have been presented by Salinger[1] and by Bullis *et al.*[2] Several properties of the low-voltage arc make it difficult to analyze theoretically. It is a high-current mode in which the ionization is produced by collision processes within the volume of the discharge and it is a highly nonlinear, nonuniform discharge having strong axial and radial variations in potential, particle densities, and temperatures. It does not exist in thermal equilibrium, but instead in a dynamic steady state governed by the interaction of several generation, loss and transport mechanisms. It operates in an intermediate pressure range, 0.5–5 Torr, in which collisions cannot be neglected, but in which the particle motion is not entirely collision dominated. The appearance of the discharge is shown in Fig. 1 for a neon-filled diode with a pressure of a few Torr, current of a few amps, and diode spacing of approximately 2 cm. In this figure, the darker the shading, the more intense is the illumination of the plasma. The low-voltage arc mode possesses an exceedingly brilliant region in the shape of an oblate spheroid adjacent to the cathode. This "cathode ball of fire" is much brighter than the conventional ball-of-fire mode. A very thin dark space exists between the cathode and the cathode ball of fire. The region toward the anode is much less intensely illuminated.

Several analytic models have been proposed to explain the behavior of the low-voltage arc. These models differ considerably in regard to the assumptions made and thus it is not surprising that the conclusions drawn are somewhat at variance. Also, all of the recent analyses have been performed for cesium low-voltage arcs which are inherently more difficult to analyze than noble-gas low-voltage arcs. All of these previous analyses have been one-dimensional and have presumed a Maxwellian electron-velocity distribution throughout the plasma region. However, there is strong evidence that this may not be true. Also, all attempts to solve the nonlinear and nonuniform transport problem have required simplifying assumptions whose effects it has been difficult to assess. Finally, the problem of determining the thermalization mechanisms has not been fully explored.

The present study involves a statistical simulation of the low-voltage arc mode on a digital computer to determine the predominant thermalization and transport mechanisms. Several different computer experiments have been used successfully in other recent studies of plasma-diode problems.[3–6] However, these previous studies have been one-dimensional, whereas for simulation of the low-voltage arc mode it has been necessary to develop a two-dimensional model.

II. FORMULATION OF THE MONTE CARLO ANALYSIS

A. General Description of the Method

The Monte Carlo analysis used in the present investigation is a self-consistent analysis similar to previous approaches in that it is largely based upon determining the motions of individual particles under the influence of the other particles in the system.

* This work was supported by the U.S. Army Electronics Command.

† Present address: Sylvania Electronic Systems, Mountain View, Calif. 94042.

[1] S. N. Salinger, Tech. Rept. No. 99, Contr. No. DA-36-039 AMC-02269(E), Electron Physics Laboratory, The University of Michigan, Ann Arbor (March 1967).

[2] R. H. Bullis *et al.*, J. Appl. Phys. **38**, 3425 (1967).

[3] P. Burger, J. Appl. Phys. **36**, 1938 (1965).

[4] J. E. Rowe and R. J. Lomax, *Proceedings of the 25th Annual Conference on Phys. Electronics* (Technology Press, Cambridge, Mass., 1965), pp. 109–120.

[5] C. M. Goldstein, in *Proceedings of the Thermionic Conversion Specialist Conference*, Cleveland, Ohio (1964), pp. 188–197.

[6] P. Burger, in *Proceedings of the Thermionic Conversion Specialist Conference*, San Diego, Calif. (1965), pp. 65–68.

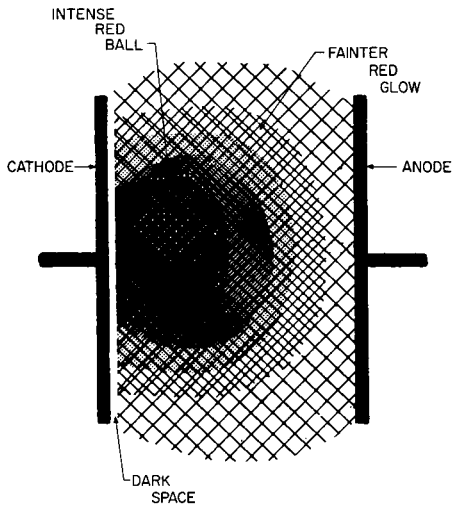

FIG. 1. Visual appearance of the low-voltage arc mode in a planar plasma diode.

A highly idealized and simplified outline of the basic flow diagram for the computer simulation is shown in Fig. 2. The procedure consists of a series of logical subroutines which are sequentially performed in a basic cycle. The various physical processes represented by these subroutines are interdependent and occur continuously and simultaneously in a real plasma diode. However, to permit computer simulation, the interdependencies between these processes must be distinguished and arranged in a cyclic sequence. For this procedure to be valid, the change in the state of the model over a single iteration must be small.

The process of following the particle motion consists of computing the electric fields in the diode on the basis of the electron distribution at a given instant, and then updating the coordinates of the electrons over a short time interval under the influence of the fields they encounter during that interval. The effects of collisions upon the electron motion are also treated in great detail. Other subroutines generate thermionic electrons at the cathode, determine currents to the boundaries and adjust the anode voltage and dc electric field. After the electron coordinates have been updated, a new charge distribution is determined and used to compute a new space-charge potential distribution and a new electric-field distribution. The particles are then updated again under the influence of the new field distribution and the process is repeated cyclically.

Initial efforts also included updating of ions along their trajectories, starting with an initial uniform ion distribution, and generation of new ions by ionizing collisions of electrons with neutral atoms. However, with the inclusion of these effects in the simulation, it was not possible to achieve stable operation and convergence of the computer program without following much larger numbers of electrons and ions than were consistent with computer storage and computation time limitations. Instead, the ion distribution was held fixed at the measured experimental distribution for the diode being simulated. Such use of the experimental ion distribution is reasonable, permits stable operation of the simulation, and saves considerable computer time over any method which includes ion drift.

The iterative process is continued until the electron distribution and the resulting potential distribution reach a steady state or until a definite instability is determined, in which event the computation is terminated. Since the electrons are tracked individually and the number of electrons that can be followed is limited, a steady state may only be approached up to the limit of statistical fluctuations of the particle distributions. Once this "statistical steady state" is reached, the electron distribution, potential distribution, and all other interesting information about the system are sampled over a number of successive iterations and these data are stored. The acquired data may then be statistically analyzed to provide estimates, within specified confidence limits, of many quantities of interest within the plasma diode.

To justify this sampling in time for a single simulation, it is necessary that all physical or mathematical stochastic processes in the Monte Carlo simulation be stationary and ergodic. The requirement of a stationary state assures that, before sampling begins, a statistical steady state has been reached in which all probability functions are invariant under a shift in the time origin. The requirement of ergodicity assures that data obtained over a long period of time from a single simulation may be interpreted in the same way as data obtained simultaneously from a large number of identical simulations at an arbitrary moment.

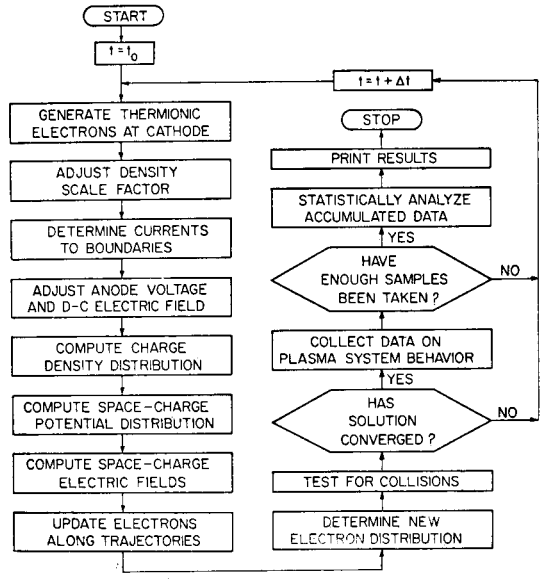

FIG. 2. Idealized schematic of basic logical flow diagram.

B. Description of the Theoretical Model

The model used in the analysis is shown in Fig. 3. It consists of a parallel-plane diode with a circular thermionic cathode. The cathode is grounded and is surrounded by a grounded guard ring. The diameters of the guard ring and anode are large compared with the cathode radius a and the diode spacing d. The diode is assumed to be filled with a noble gas at pressure p, and there is no applied magnetic field. The discharge current is designated as I, and the discharge voltage is designated as V_a.

The problem is treated in cylindrical coordinates, and axial symmetry is assumed so that there is no variation in the θ direction. It is then adequate to consider only a sector of the diode of depth $\Delta\theta$ in the θ direction. Also, there is, on the average, no net force on any particle in the θ direction.

The major assumptions not already mentioned are as follows:

(1) Nonrelativistic mechanics is used.
(2) The gas is weakly ionized.
(3) Collisions between charged particles may be neglected. The coupling mechanism between charged particles comes from the space-charge fields.
(4) The time steps taken are short enough that the instantaneous state of the system undergoes only a perturbational change from iteration to iteration.
(5) The gas pressure is sufficiently high so that collisions damp out any large-amplitude plasma oscillations.
(6) In collisions of electrons with neutral atoms, the scattering is isotropic.
(7) The electron emission from the cathode is space-charge limited and is uniform over the surface of the cathode.
(8) The only electron–neutral collision processes included are elastic collisions and ionizing collisions.

When operated in the low-voltage arc mode, a plasma diode exhibits a very steep current–voltage characteristic, with large changes in current producing only slight changes in voltage. In fact, for stable operation in this mode it is generally necessary to use a current-regulated power supply or a large current-limiting resistor in series with the diode. To obtain a realistic simulation, the model was therefore supplied with a constant current source, and current was taken as an independent variable. (This also provided a means for controlling the anode potential by comparing the instantaneous anode current due to computer electrons crossing the anode boundary with the desired anode current, and then modifying the anode voltage to drive the current toward the desired value.)

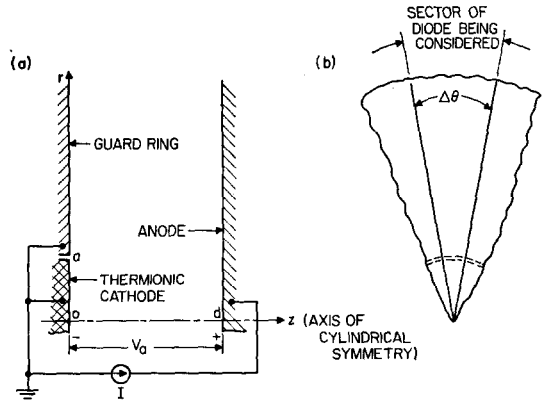

FIG. 3. Model of the diode used in the analysis.

C. Motion of Electrons

The equations of motion of the electrons may be readily obtained by numerically integrating the force equations. The axial velocity component and position of an electron at time $t_{l+1}=t_l+\Delta t^-$ are given by

$$\dot{z}(t_{l+1})=\dot{z}(t_l)-\eta E_z(t_l)\,\Delta t^- \tag{1}$$

and

$$z(t_{l+1})=z(t_l)+\tfrac{1}{2}[\dot{z}(t_l)+\dot{z}(t_{l+1})]\Delta t^-, \tag{2}$$

where $\eta=e/m$ and $E_z(t_l)$ is the z component of the electric field seen by the electron at time t_l. Similar expressions are used for $\dot{r}(t_{l+1})$ and $r(t_{l+1})$.

The kinetic energy $\mathcal{E}(t_{l+1})$ may be obtained by eliminating the θ-velocity components from the expressions for $\mathcal{E}(t_{l+1})$ and $\mathcal{E}(t_l)$ in terms of their velocity components under the condition that $v_\theta(t_l)=v_\theta(t_{l+1})$. The result is

$$\mathcal{E}(t_{l+1})=\mathcal{E}(t_l)+(1/2\eta)\{[2\dot{z}(t_l)+\Delta\dot{z}]\Delta\dot{z}+2[\dot{r}(t_l)+\Delta\dot{r}]\Delta\dot{r}\}, \tag{3}$$

where $\Delta\dot{z}=\dot{z}(t_{l+1})-\dot{z}(t_l)$ and similarly for $\Delta\dot{r}$.

The probability that an electron of energy $\mathcal{E}$ will undergo a collision of type k in an interval Δt^- is given by

$$P_k'(\mathcal{E},\Delta t^-)=1-\exp[-\nu_k(\mathcal{E})\,\Delta t^-], \tag{4}$$

where $\nu_k(\mathcal{E})$ is the collision frequency. The probability of an electron surviving a time Δt^- without undergoing any type of collision is given by

$$P_0'(\mathcal{E},\Delta t^-)=\exp[-\Delta t^-\sum_{k=1}^{L}\nu_k(\mathcal{E})], \tag{5}$$

where L is here the number of types of collisions considered.

Considering only elastic and ionizing collisions, the sum of the probabilities of the various events is

$$P_0'(\mathcal{E},\Delta t^-)+P_E'(\mathcal{E},\Delta t^-)+P_I'(\mathcal{E},\Delta t^-)=1+P_S'(\mathcal{E},\Delta t^-), \tag{6}$$

where $P_0'(\mathcal{E},\Delta t^-)$ is defined in Eq. 5; $P_E'(\mathcal{E},\Delta t^-)$ and $P_I'(\mathcal{E},\Delta t^-)$ are, respectively, the probabilities that an electron of energy $\mathcal{E}$ will undergo an elastic or ionizing collision in an interval Δt^-, as given in Eq. 4, and

$P_S'(\mathcal{E}, \Delta t^-)$ is the joint probability of an electron undergoing both an elastic and ionizing collision during Δt^-. To determine the occurrence of a collision, it is convenient to normalize the probabilities on the left so that their sum is unity. To do this, define

$$P_k'' = P_k'(\mathcal{E}, \Delta t^-)/[1+P_S'(\mathcal{E}, \Delta t^-)], \qquad k=0, E, I. \tag{7}$$

In practice, it is necessary to choose Δt^- short enough that there is a negligible probability of an electron undergoing more than one collision during Δt^-. Then $P_S'(\mathcal{E}, \Delta t^-) \ll 1$ and $P_k'' \approx P_k'(\mathcal{E}, \Delta t^-)$.

Next, generate a random number R_C, uniformly distributed on $0 \leqq R_C \leqq 1$, and test R_C as follows. If $0 \leqq R_C < P_0''$, then no collision occurs; if $P_0'' \leqq R_C < P_0''+P_E''$, an elastic collision occurs; if $P_0''+P_E'' \leqq R_C \leqq 1$, an ionizing collision occurs.

If it is decided that a given electron has undergone a collision during the interval Δt^-, then its velocity components and energy must be appropriately adjusted. For simplicity, the scattering is assumed to be isotropic. Also, it is assumed that, after scattering, the θ component of the electron's motion always gets its average fraction of the remaining energy, i.e., one-third. If $\mathcal{E}'$ is the kinetic energy remaining after the collision, the velocity components after the collision are then related to the energy by

$$\dot{z}'^2+\dot{r}'^2=\tfrac{2}{3}(2\eta\mathcal{E}'). \tag{8}$$

For the scattering to be isotropic, it is necessary that all values of the angle ψ, which the component of the velocity vector in the z–r plane makes with the z axis, be equally probable. This leads to a cumulative distribution function for ψ of $G(\psi)=\psi/2\pi$. A random number R_1, uniformly distributed on $0 \leqq R_1 \leqq 1$, is generated and equated to $G(\psi)$, yielding $\psi=2\pi R_1$. Relating ψ to $\dot{z}'$ and $\dot{r}'$, and inserting numerical values then yields

$$\dot{r}'=4.8427\times10^5(\mathcal{E}')^{1/2}\sin 2\pi R_1, \quad \text{m/sec} \tag{9}$$

and

$$\dot{z}'=4.8427\times10^5(\mathcal{E}')^{1/2}\cos 2\pi R_1, \quad \text{m/sec.} \tag{10}$$

If the electron undergoes an ionizing collision a new electron must be generated at the point of the collision. The energy to be shared between the primary and secondary electrons immediately after the collision is $\mathcal{E}-\mathcal{E}_I$, where $\mathcal{E}_I$ is the threshold energy for ionization. It is assumed that this energy is uniformly and randomly shared between the two electrons with equal probability. The kinetic energy of the primary electron is then taken as $\mathcal{E}'=R_3(\mathcal{E}-\mathcal{E}_I)$, while that of the secondary electron is taken as $\mathcal{E}''=(1-R_3)(\mathcal{E}-\mathcal{E}_I)$, where R_3 is a random number. The velocity components of the two electrons are then assigned in the manner of Eqs. (9) and (10).

In an elastic collision with a neutral atom, the mean fractional energy loss of an electron is in the range of 10^{-4} to 10^{-5}. In a plasma which is collision dominated, or nearly so, elastic collisions occur frequently enough for this small fractional energy loss to become an important thermalization mechanism. However, since a computer simulation cannot be run nearly long enough for these small electron-energy losses to have a significant cumulative effect, these losses are neglected, and it is assumed that $\mathcal{E}' \cong \mathcal{E}$. Thermalization within the computer model is brought about by randomization of the electron directional distribution in elastic collisions coupled with randomization of electron energy in the fluctuating electric field of the tracked electrons themselves. Initial operation of the program using elastic collision frequencies based upon published collision cross section data failed to provide sufficient thermalization using this method to assure stable operation and convergence. However, an increase in the collision frequency by a factor of ten to simulate the effect of the necessary, but missing, thermalization mechanism did lead to stability and convergence. The number of possible candidates for this predominant thermalization mechanism was reduced to recoil loss in elastic collisions, as discussed above, and some form of collective charged particle interaction such as the growth and breakup of local plasma instabilities with characteristic wavelengths less than the minimum resolvable distance in the computer model. In future calculations it is anticipated that a smaller grid size can be utilized so that local plasma oscillations can be included as a thermalization mechanism. There is no fundamental limitation to the inclusion of these mechanisms; only limitations on computer time.

D. Determination of Charge Densities, Space-Charge Potentials, and Electric Fields

To determine the spatial variation of the electron densities, the diode is divided into cells and, at each iteration, the number of tracked electrons in each cell is counted. Sample estimates of the net charge densities in each of the cells are then given by

$$\rho_{i,j}=(e/Y_{i,j})(n_{i,j}^+-B_n^-N_{i,j}^-). \tag{11}$$

Here $n_{i,j}^+$ is the experimentally determined ion density in cell (i, j); $N_{i,j}^-$ is the number of tracked sample computer electrons in cell (i, j); B_n^- is the electron-density scale factor, i.e., the number of physical electrons in the total population of the volume under consideration that each sample computer electron represents, and $Y_{i,j}$ is the volume of cell (i, j).

Due to the limited number of particles that can be tracked on the computer, there will be a relatively small number of computer particles of each species in each cell, and so taking the difference in Eq. (11) may lead to large fluctuations and unrealistically high values for the $\rho_{i,j}$'s. To smooth out these fluctuations and bring the $\rho_{i,j}$'s down to realistic magnitudes, two steps are taken. First, the electron density in each cell is

replaced by the average of the electron densities of that cell and the eight surrounding cells, thereby spreading the charge of each computer electron over a nine-cell region and reducing the fluctuations at the expense of a reduction in resolution of the electron density. Next, the smoothed charge density is multiplied by a space-charge reduction factor β_{sc} which reduces the estimated net charge density to that value required to bring the instantaneous peak potential within the diode, V_{pk}, into agreement with a specified experimental value of V_{pk}. A feedback loop is used to regulate β_{sc}, and hence, V_{pk} at the correct value.

With an estimate of the charge-density variation, it is possible to solve Poisson's equation to obtain the space-charge potential variation. The boundary-value problem to be solved is

$$\partial^2\varphi/\partial z^2+\partial^2\varphi/\partial r^2+(1/r)\partial\varphi/\partial r=-\rho(z,r)/\epsilon_0,$$
$$0\leqq z\leqq d,\ 0\leqq r\leqq\infty, \quad (12)$$
$$\varphi(0,r)=\varphi(d,r)=0, \qquad 0\leqq r\leqq\infty, \quad (13)$$
$$\varphi(z,\infty)=0, \qquad 0\leqq z\leqq d, \quad (14)$$
$$\partial\varphi/\partial r=0 \quad \text{at} \quad r=0,\infty, \qquad 0\leqq z\leqq d. \quad (15)$$

Since this problem must be solved hundreds of times during the course of the computation, it is necessary to use the fastest possible method of solution. The method used is a combination of Fourier analysis and the marching method,[7,8] as adapted to cylindrical coordinates. The details of the analysis may be found in Ref. 1.

In this method, the boundary conditions (14) and (15) at $r=\infty$ are approximated at a finite distance $\hat{r}$ by taking $\varphi(\hat{r}+\Delta r)=\gamma\varphi(\hat{r})$, where γ is an appropriately determined constant. This method approximates the infinite region $r\geqq 0$ by the bounded region $0\leqq r\leqq\hat{r}$, and permits discarding of computer electrons which cross the radial boundary $r=\hat{r}$. With 48 radial cell divisions this led to an average error in computed potential of 0.51% and an average error of only 0.13% over the inner 39 cells. Once the array of potentials is known, the electric fields are obtained by differentiating the potentials using finite-difference methods.

E. Generation and Loss Mechanisms

To determine the currents crossing the various boundaries it is necessary at each iteration of the simulation to count the number of electrons crossing these boundaries. Prior to updating each electron, the coordinates of the electron are tested to see if it has crossed any of the boundary planes and left the diode. If it has, a count is registered for the appropriate boundary plane, the electron is eliminated from storage in the computer memory, and the next electron is considered. If, on the other hand, the electron lies within the boundaries, it is updated in the usual fashion.

The electron current to the anode is given by

$$I_b^-=eB_n^-\langle N_n^-\rangle_{av}/[\Delta t^-(\Delta\theta/2\pi)], \quad (16)$$

where $\langle N_b^-\rangle_{av}$ is the mean number of computer electrons reaching the anode plane, averaged over several iterations. The factor $\Delta\theta/2\pi$ is the fraction of the total anode surface to which the sector under analysis of the diode corresponds, and is thus the fraction of the electron current which enters the anode through $\Delta\theta$. The discharge current I is approximated by the electron current to the anode, so that $I\approx I_b^-$.

Next consider the thermionic emission of electrons from the cathode. In the low-voltage arc mode the emission is space-charge limited, and it is estimated that the distance from the cathode to the potential minimum is of the order of 10^{-4} cm. On the other hand, the diode spacing is of the order of 2 cm, so that for an axial resolution of 48 cells the distance to the first grid point off the cathode is of the order of 10^{-2} cm. Therefore, the detailed variation of the potential distribution in the neighborhood of the potential minimum cannot be resolved, so that the detailed particle motion involved in the space-charge-limiting process cannot be simulated.

The approach that is followed is to generate at the cathode at each iteration a number of electrons corresponding to the space-charge-limited current. The emitted electrons are effectively coming from the potential minimum, but negligible error is introduced by assuming that the virtual cathode at the potential minimum coincides with the real cathode. The required number of electrons is

$$\langle N_{em}^-\rangle_{av}=(\Delta\theta\Delta t^-/2\pi eB_n^-)I+\langle N_e^-+N_d^-\rangle_{av}. \quad (17)$$

Here, the first term on the right supplies the number of electrons corresponding to the desired discharge current reaching the anode. The second term balances those electrons lost by backscattering from the plasma to the cathode plane and by radial diffusion.

The electrons are generated with zero initial energy and velocity components, since these initial values are negligible compared with the values attained after the electrons are accelerated through the cathode sheath. The probability density function for the radial coordinates of the emitted electrons is taken to be proportional to $r\Delta\theta$ to assure uniform emission over the surface of the cathode. A similar procedure is used for controlling the anode potential by comparing the instantaneous anode current with the desired anode current.

A necessary requirement is the adjustment of the density-scale factor B_n^-. As the simulation approaches a steady state, the number of tracked electrons may tend to exceed the allowable upper bound. Whenever

[7] R. W. Hockney, Rept. No. SU-SEL-64-056, Stanford Electronics Laboratories, Stanford University, Stanford, Calif. (May 1964).

[8] R. P. Wadhwa and G. Kooyers, Rept. No. NASA CR-54033, Electron Tube Division, Litton Industries, San Carlos, Calif. (1964), pp. 87–104.

this occurs, a randomly selected fraction of the tracked electrons, say 3%, is eliminated from storage and discarded. At the same time, the density-scale factor is increased by the same fraction to properly increase the weights of the remaining tracked electrons that have not been eliminated. Since the elimination is done randomly, no bias is introduced by this process. However, it does tend to preferentially enhance the fluctuations in the low-density regions. To overcome this would require an important sampling scheme which combines a spatially varying B_n^- with nonuniform elimination probabilities.

F. Estimation of Plasma Parameters

To terminate the computation it is necessary to specify suitable convergence criteria for the simulation. Due to the complexity of the model, the specification of adequate numerical criteria is difficult. In practice, it is found most convenient to visually monitor a large number of printed output variables from iteration to iteration. When it is judged that the mean values of these variables have adequately leveled off, and all that remain are statistical fluctuations about the means, the simulation is considered to have converged. Additional iterations are then run during which data are collected for statistical analysis. These data are then used to estimate mean values and confidence limits for all physical quantities of interest.

In the statistical analysis the sample mean and standard error of the sample mean are computed for each estimated parameter of interest. These are then used to compute confidence bands for the spatial variations of the estimated parameters. Since much data are collected during each sampling iteration, and the computation time during each sampling iteration is lengthy, data collection, storage, and processing considerations limit the number of sampling iterations to around 100. Consequently, Student's t statistics are used to eliminate biases in the estimates of confidence bandwidths due to small-sample effects. In addition, sampling over successive iterations causes a degree of correlation between successive samples since the electron-updating procedure is a Markov process in which the successive steps are not statistically independent of one another. The effect of this correlation is also considered in the computation of confidence bands, since the correlation increases the width of the confidence interval by increasing the standard error.

This analysis is used for computing the means for several arrays of plasma variables. The confidence intervals are computed for selected rows of these arrays. The sample mean of the electron density in cell (i, j) is given by $\langle n_{i,j}^- \rangle_{\text{av}} = (B_n^-/Y_{i,j})\langle N_{i,j}^- \rangle_{\text{av}}$, where $\langle N_{i,j}^- \rangle_{\text{av}}$ is the sample mean of the number of computer electrons in cell (i, j) and $Y_{i,j}$ is the volume of the cell. The sample means of the potentials at each grid point are estimated from the sum of the space-charge potential and d-c potential at each mesh point as $\langle V_{i,j} \rangle_{\text{av}} = \langle \varphi_{i,j} \rangle_{\text{av}} + (i/K)\langle V_a \rangle_{\text{av}}$. By differentiating the potential distribution, the electric-field intensity may be determined. Also, by recording the location of every ionizing collision occurring during the sampling iterations following convergence, the mean number of computer ionizations per iteration $\langle Z_{i,j} \rangle_{\text{av}}$ may be determined. The sample mean ionization rate per unit volume per second is then given by $\langle \zeta_{i,j} \rangle_{\text{av}} = \langle Z_{i,j} \rangle_{\text{av}} B_n^+ / Y_{i,j} \Delta t^+$. Sample means and confidence intervals are also determined for the currents to the boundaries.

Next it is necessary to estimate the electron temperature and energy density function. The "temperature" used here is defined by the relation

$$e\langle \mathcal{E} \rangle_{\text{av}} = \tfrac{1}{2} m \langle v^2 \rangle_{\text{av}} \tfrac{3}{2} k T^-. \tag{18}$$

This definition differs from the usual kinetic theory definition, in which $m\langle (v-\bar{v})^2 \rangle_{\text{av}}/2 = 3kT^-/2$, in that it includes the translatory kinetic energy of the electrons. The mean velocity is omitted from the definition (18) because inclusion of this term would require the collection, storage and reduction of data on the individual velocity components of each electron, in addition to the electron energies, thereby tripling the data to be processed for the computation of temperatures. In regions where the electron distribution is reasonably well thermalized, the drift energy is presumed to be small compared to the thermal energy, and the neglect of $\bar{v}$ in Eq. (18) introduces little error. In nonthermalized regions, where $\bar{v}$ is not small, Eq. (18) yields a higher temperature than the customary definition. With either definition, the concept of a temperature loses much of its usefulness and significance in regions having significant drift velocities or anisotropies because the information concerning these latter processes is lost in the averaging process. To emphasize the distinction between the present definition of temperature and the usual kinetic theory definition, the quantity T^- defined by Eq. (18) will be referred to as a "pseudoelectron temperature." Using Eq. (18), the sample mean pseudoelectron temperature in cell (i, j) is given by $\langle T_{i,j}^- \rangle_{\text{av}} = 7737 \langle \mathcal{E}_{i,j} \rangle_{\text{av}}$, °K, where $\langle \mathcal{E}_{i,j} \rangle_{\text{av}}$ is the mean electron energy in cell (i, j) expressed in eV.

To estimate the electron energy density function, $f(\mathcal{E}, z)$, the diode is divided into groups of cells along the z axis, and then the electrons in each cell group during the sampling iterations are sorted into energy classes. The mean fraction $\langle \kappa_{k,m} \rangle_{\text{av}}$ of the electrons in cell group k which are in energy class m is then computed for each pair (k, m). The mean fraction of electrons per unit energy interval is then given by $\langle f_k(\mathcal{E}_m) \rangle_{\text{av}} = \langle \kappa_{k,m} \rangle_{\text{av}} / (\Delta \mathcal{E}_m)$, where $(\Delta \mathcal{E})_m$ is the width of the mth energy class, centered about energy $\mathcal{E}_m$. The products $\langle n_{i,j}^- \rangle_{\text{av}} \langle f_k(\mathcal{E}_m) \rangle_{\text{av}}$, where cell (i, j) is centered within cell group k, provide sample estimates of the axial variation of $f(\mathcal{E}, z)$.

III. SIMULATION AND ANALYSIS OF A NEON LOW-VOLTAGE ARC

A. Specification of Operating Conditions

The discharge to be simulated is a neon low-voltage arc operating under the conditions $p=2$ Torr, $I=4$ A, and $d=2.37$ cm. The cathode radius is $a=0.889$ cm, and the cathode temperature is sufficiently high to assure space-charge-limited operation. The neutral gas temperature is estimated to be $T=300°K$. This particular operating point was chosen to make use of and provide a comparison with Martin's[9] extensive Langmuir-probe data under these conditions. Pulsed and shielded Langmuir-probe data for the spatial variations of the plasma potential, electron density, and electron temperature, obtained by Martin, are shown in Fig. 4 for the stated operating conditions. Data of this type are

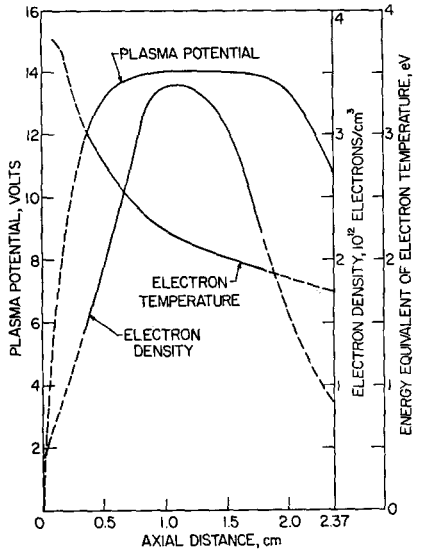

FIG. 4. Experimental behavior of the plasma diode being simulated. Axial profiles of plasma potential, electron density, and electron temperature. Operating conditions: neon at $p=2$ Torr, $I=4$ A, and $d=2.37$ cm. (from Martin[9]).

used to estimate an initial state of the system from which to begin computations. Other reasons for choosing this particular operating point are that it is known to be stable and that complete atomic collision data are available for neon.

In this simulation, 10 000 particles of each species (i.e., electrons and ions) were tracked, and a 48 by 49 cell array was chosen for the computation of potentials. The optimum electron updating interval was found to be $\Delta t=2\times10^{-10}$ sec. Somewhat arbitrarily, $\Delta\theta$ was taken as 10^{-6} rad, leading to density scale factors of the order of 300. Data were collected for analysis over 150 updating iterations after convergence was reached.

[9] R. J. Martin, Tech. Rept. No. 101, Contr. No. DA-36-039 AMC-02269(E), Electron Physics Laboratory, The University of Michigan, Ann Arbor (June 1967).

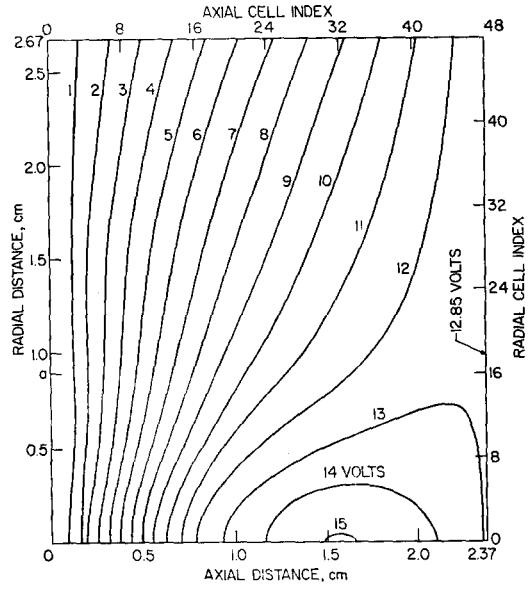

FIG. 5. Contours of constant potential, (V).

B. Results of the Analysis and Conclusions

The results of the analysis are presented as a series of contour plots and parametric curves of the computed behavior of the plasma properties. The presented curves are the result of smoothing the curves obtained directly from the computer. The latter curves contained many fluctuations about the reduced smooth curves.

Figure 5 shows the computed contours of constant potential in the discharge, while Fig. 6 shows the confidence intervals for the axial variation of the potential as a function of radial cell index. In these figures, the potential peak near the center of the discharge is clearly displayed. This peak occurs somewhat closer to the anode than is observed experimentally, and the cathode fall of potential is not as steep as in

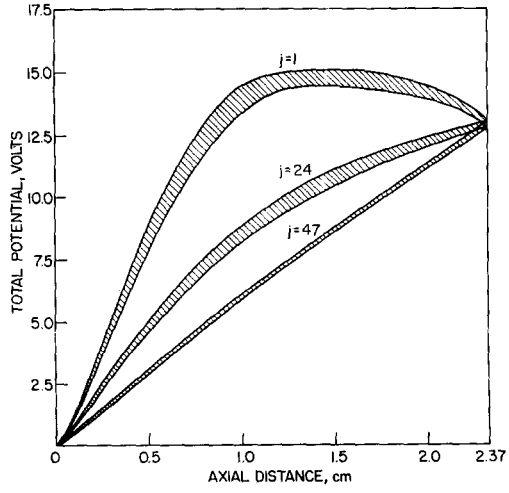

FIG. 6. Ninety-percent confidence bands for the axial variation of the total potential as a function of radial cell index.

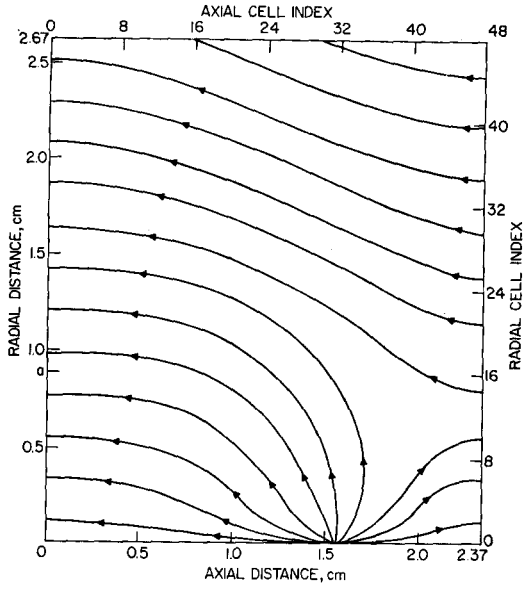

FIG. 7. Contour plot of electric field lines.

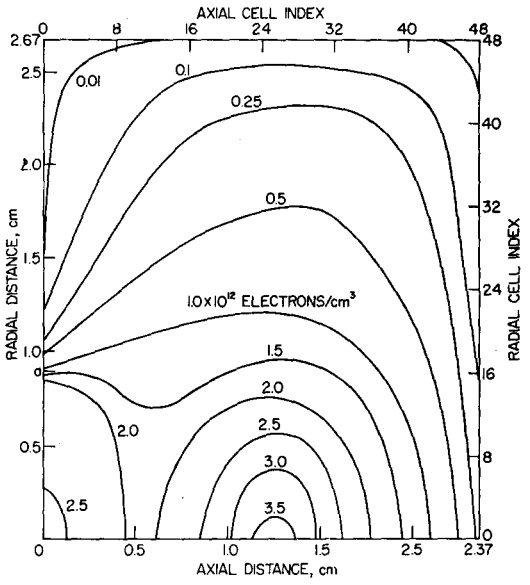

FIG. 9. Contours of constant electron density, (electrons/cm³).

experimental observations. This discrepancy will be discussed shortly. It is also seen that the space-charge component of the total potential decreases rapidly with increasing radial distance, so that the total potential approaches a ramp function due to the applied dc potential. An anode fall of potential exists only near the center of the anode where the space-charge electric field predominates over the applied dc electric field. On the radially distant parts of the anode where the situation is reversed, there is no anode fall of potential; the potential rises monotonically to the anode voltage.

Figure 7 shows the electric field lines which indicate the directions along which ions in the real discharge drift due to mobility effects. It is evident that most of the ions generated within the central high-potential region eventually reach the cathode plane, while only a small fraction drift toward the anode. It is also evident that diffusion must play a major role in permitting ions to move across the field lines to radially distant regions not directly connected by field lines to the high-potential region where most of the ions are generated.

Figure 8 shows a contour plot of curves of constant $|E|/p$. This ratio is a measure of the mean energy acquired by the ions from the electric field. The locations of the cathode double sheath and anode fall of potential are clearly displayed. Nowhere in the discharge is the electric field strength sufficiently low for the condition $|E|/p \ll 2$ V/Torr·cm to be valid. This

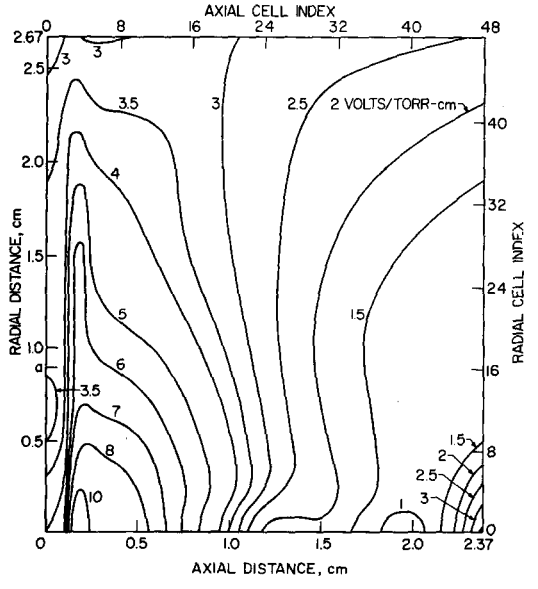

FIG. 8. Contour plot of $|E|/p$, (V/Torr·cm).

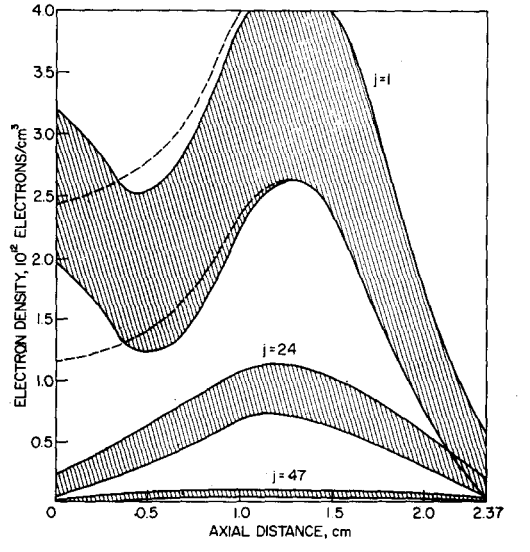

FIG. 10. Ninety-percent confidence bands for the axial variation of the electron density as a function of radial cell index.

is the criterion suggested by McDaniel[10] for the validity of using an analysis employing constant ionic mobility, independent of the field strength. Thus, the high $|E|/p$ values shown in Fig. 8 suggest that any transport analysis of the low-voltage arc mode, which includes the effect of ion drift, should employ an electric-field-dependent ion mobility. The strong electric fields also suggest that the electron drift velocities are nonnegligible throughout most of the discharge, so that the neglect of $\bar{v}$ in the definition of temperature is not well justified. Future treatments should permit the gathering of electron velocity data for a more rigorous treatment of electron temperature.

Figure 9 shows the computed contours of constant electron density in the discharge. A peak in the electron density occurs at the center of the discharge with rapid decreases in the density occurring radially and axially toward the anode. However, a strong secondary maximum also occurs at the cathode, in disagreement with experiment. Figure 10 shows the 90% confidence bands for the electron densities $n^-(z, r_j)$. Percentagewise, the greatest uncertainties in the estimated electron density occur for both very large and very small j. This is because the real electron density decreases radially, while the cell volume increases radially, producing maximum concentrations of computer electrons at intermediate radial distances.

It is believed that the discrepancy between the computed and experimental profiles for both the electron density and electric potential arise from a combination of inaccuracy of the experimental ion density profiles in the neighborhood of the cathode and the inability of the computer program to correct for this inaccuracy by a self-consistent inclusion of diffusion and drift of the ions in the simulation. In the cathode ball-of-fire region, the measured ion densities were accurate to at most only ±20%, and measurements on the central axis were not made closer than 0.5 cm to the cathode. It is possible that the ion density near the cathode falls to only 1.5×10^{12} ions/cm³ rather than the 0.4×10^{12} ions/cm³ indicated in the extrapolation in Fig. 4. This increased ion density near the cathode would raise the potential there and narrow the computed cathode fall space. The steeper cathode fall would, in turn, accelerate thermionic electrons away from the cathode more rapidly and eliminate the secondary maximum of electron density at the cathode. The confidence band for estimated electron densities on the axis at the cathode would then be lowered and would appear somewhat like the dashed lines in Fig. 10. If it had been possible to include drift and diffusion of the ions into the simulation, the initial ion distribution and the electron and potential distributions would all have been corrected in an internally consistent manner. A proposed, but as yet untested, method for the inclusion of ion drift and diffusion in the computer simulation of a gas discharge is outlined in the Appendix.

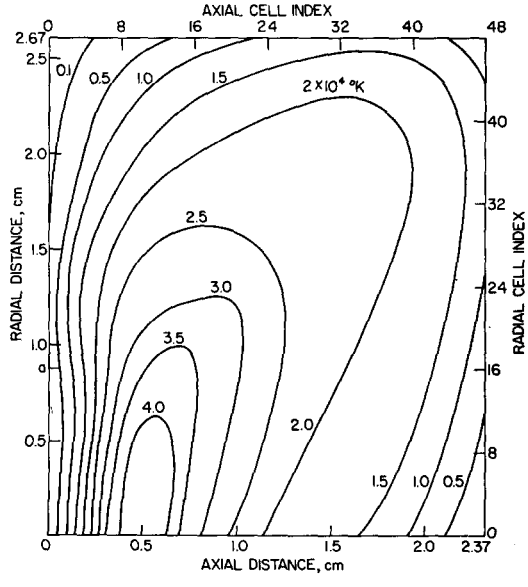

FIG. 11. Contours of constant pseudoelectron temperature, (°K).

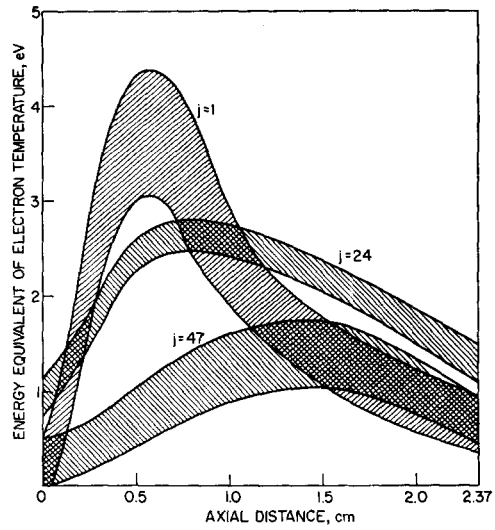

FIG. 12. Ninety-percent confidence bands for the axial variation of the electron pseudotemperature as a function of radial cell index.

Ninety-percent confidence intervals were also determined for the electron currents to the boundaries. The anode current was in the range $1.2<I_b^-<2.1$ A, the radial diffusion current was in the range $1.0<I_d^-<1.4$ A, and the electron current backscattered to the cathode plane from the plasma was in the range $0.48<-I_c^-<0.78$ A. The anode voltage was in the range $12.7<V_a<13.0$ V.

The observed anode current was somewhat lower than expected, while the observed radial diffusion current was somewhat higher than expected. These results, coupled with the observed behavior of the

[10] E. W. McDaniel, *Collision Phenomena in Ionized Gases* (John Wiley & Sons, Inc., New York, 1964), p. 437.

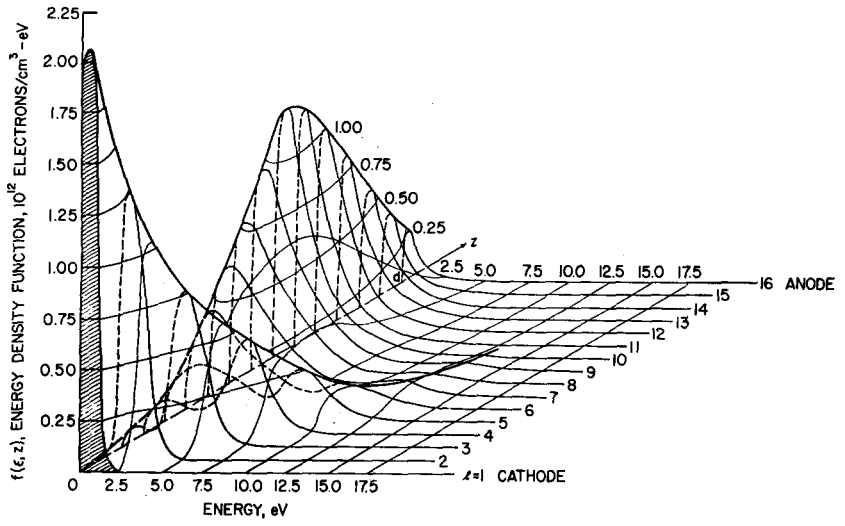

FIG. 13. Relief plot of the electron-energy density function along the z axis.

electric fields and a comparison of the model geometry with Martin's experimental plasma diode, yield an important conclusion as to the nature of the electron transport mechanism in the low-voltage arc mode. Since the anode current was determined on the basis of the electrons striking the anode at radial distances of $r<\hat{r}=2.67$ cm, while the radius of the anode in Martin's experimental diode was 5.08 cm, it appears that a sizable fraction of those electrons, which would have struck the anode and contributed to the current, crossed the boundary $r=\hat{r}$ and were eliminated from the computer's memory before they could reach the anode and contribute to the current. The following theory of electron transport to the anode then emerges.

Electrons entering the plasma from the cathode are accelerated along the inward-curving field lines toward the high-potential region where they may undergo exciting and ionizing collisions. A strong radial electron density gradient forms, across which an outward radial electron diffusion current develops. In addition, electrons may diffuse radially while they are being accelerated away from the cathode, and sizable numbers may never even enter the high-potential region. As these electrons diffuse radially outward, they encounter electric fields which cause them to simultaneously drift toward the anode. Thus, the path of least resistance for electrons to reach the anode is not to climb down the anode fall of potential, but rather to diffuse radially to where there is no anode fall of potential and where they may drift toward the anode in a prevailing accelerating electric field. This mechanism permits large numbers of electrons, with energies which are much less than those required for climbing down the anode fall of potential, to reach the anode, thereby permitting a much larger current to flow than is predicted by one-dimensional theories assuming a uniform anode sheath.

The computed behavior of the electron pseudotemperature is shown in Figs. 11 and 12. A strong maximum is seen to occur on the z axis in front of the cathode, in agreement with experiment. The rise in temperature from the cathode to the peak is due to the gain in kinetic energy of the primary thermionic electrons as they are accelerated through the cathode double sheath. The fall in temperature from the peak to the anode is due to the thermalization of the electrons within the plasma as an increasing fraction of the high-energy primary electrons is converted to low-energy "ultimate" electrons. As discussed previously, the pseudotemperatures computed here are somewhat higher than those that would be obtained from the usual kinetic theory definition of temperature.

Figure 13 presents a relief plot of the electron-energy density function $f(\mathcal{E}, z)$ along the z axis. In this figure, the process of thermalization is clearly displayed. At the cathode, $f(\mathcal{E}, z)$ is a narrow-peaked, Gaussian-like distribution with its center at the energy equivalent of the total potential. This shows that most of the electrons here are in a beam moving away from the cathode and being accelerated by the cathode fall of potential. The spread in the energy distribution about the peak is due to the effects of space-charge interactions and collisions with neutral atoms upon the beam of thermionic electrons.

As this beam of electrons moves away from the cathode into regions of higher potential, the center energy of the peak increases, while the amplitude of the peak decreases and the width of the energy distribution about the peak increases. Simultaneously, another peak begins to grow at a much lower energy in the neighborhood of 1 or 2 eV. This low-energy peak is due to the thermalized electrons within the plasma. The thermalized distribution grows as the center of the plasma is approached, while the high-energy peak decreases as an increasing fraction of the primary beam electrons is thermalized. The thermalized part of the distribution clearly displays a Maxwellian form. In the region where the high-energy tail becomes negligible, the amplitude of the Maxwellian distribution is propor-

tional to the electron density, which exhibits a peak near the center of the discharge and decreases toward the anode.

It is seen that the dissipation of the cathode electron beam and the transition to a Maxwellian distribution is quite gradual, with the high-energy peak being detectable more than halfway into the plasma. In the cathode double sheath region the distribution is strongly doubled-humped, which suggests the existence of strong beam–plasma interactions tending to aid in the dissipation and thermalization of the primary beam. It is concluded that, although recoil in collisions with neutral atoms is the main thermalization mechanism in the central portion of the discharge, the growth and breakup of microinstabilities arising from the beam–plasma interactions provide the main thermalization mechanism for dissipation of the primary beam in the cathode double sheath. Although it has long been known that these interactions provide the primary thermalization mechanism in low-pressure discharges, it must here be concluded that they are also important in discharges at pressures up to 10 Torr, such as the low-voltage arc.

Ninety-percent confidence bands for $f(\mathcal{E}, z)$ are shown in Fig. 14. Even though the computed behavior of $f(\mathcal{E}, z)$ was obtained under the conditions of a fixed ion distribution, it is expected that with the inclusion of ion updating in the model and the consequent narrowing of the cathode double sheath, as discussed previously, the behavior of $f(\mathcal{E}, z)$ will remain qualitatively the same as in Fig. 14. The major modification would be a shift of the thermalized peak toward the cathode with a resultant axial compression of the double sheath and thermalization region. The dissipation of the primary electron beam would then be somewhat more rapid than is indicated in Fig. 13.

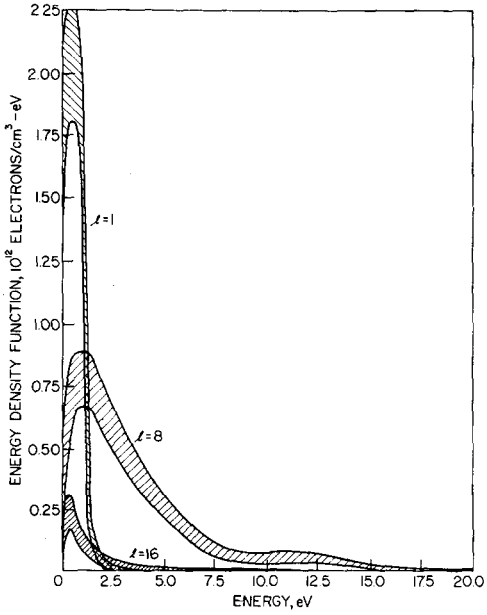

FIG. 14. Ninety-percent confidence bands for the electron-energy density function for selected cell groups along the z axis.

Finally, data were collected on the spatial distribution and rate of occurrence of ionizing collisions of electrons with neutral atoms. However, so few ionization events occurred during the sampling iterations that a meaningful estimate of the ionization rate was impossible. This is attributed to a very low concentration of electrons with sufficient energy to undergo ionizing collisions, as is verified by the electron energy density function of Fig. 13. Those ionizing collisions that did occur were confined to a region near the center of the discharge, corresponding to where the last remnant of the primary electron beam has its highest energy and widest energy spread prior to its being completely dissipated in the plasma. However, since the peak beam energy in this region is still well below the ionization potential, it is concluded that the ionization is produced by electrons in the high-energy tail of the quasi-Maxwellian distribution which exists in this region.

ACKNOWLEDGMENTS

The authors gratefully acknowledge the significant contributions of Howard Bond who programmed the problem for solution on The University of Michigan IBM-7090 digital computer. The University also supported a major portion of the computing time necessary to obtain the final results.

APPENDIX

In this Appendix, a method is proposed for the inclusion of ion drift and diffusion in the computer simulation of a gas discharge. Since the positive ions are much more massive than the electrons, they accelerate much more slowly, and under the influence of a given electric field they take much longer to travel a given distance than do the electrons. As a result, if the ions are updated in time steps that are proper for electrons, the number of iterations that would be needed to reach a statistical steady state would be prohibitively large. On the other hand, if electrons are updated in time steps that are proper for following the motion of ions, the electrons would travel so far each time step that electron trajectory calculations and the statistical analysis of the electron distribution would be meaningless.

The approach suggested for circumventing this difficulty is to use a short updating interval Δt^- for the electrons and a longer updating interval Δt^+ for the ions, with each distribution being held fixed while the other is updated. The lengths of the time steps are chosen to move the particles of each species an optimum distance in accordance with the requirements of having only perturbational changes and of reaching convergence in a minimum number of iterations. The validity of the method rests upon the assumptions

that the motion of an ion during an electron-updating interval Δt^- may be neglected and that the statistical properties of the ensemble of electrons change by a negligible amount during an ion-updating interval Δt^+. Thus, although a real electron would travel a great distance during the interval Δt^+, if the electron distribution is reasonably close to the steady-state distribution the macroscopic spatial electron distribution does not appreciably change. At the end of the interval Δt^+, each electron that was being observed at the start of the interval is considered to be replaced by a statistically equivalent electron with the same phase-space coordinates at the end of Δt^+ that the original electron had at the beginning of Δt^+.

The net motion of a computer ion in the z direction during Δt^+ may be decomposed into a component Δz_{drift} due to drift in the electric field and a component Δz_{diff} due to diffusion. Thus, the z coordinate following the kth updating interval is

$$z(t_{k+1})=z(t_k)+\Delta z_{\text{drift}}+\Delta z_{\text{diff}}, \tag{19}$$

with a similar expression for the r coordinate.

During the ion-updating interval Δt^+ there will be a high probability that an ion will undergo many collisions with gas atoms so that its motion may be taken to be mobility limited. Experimental measurements of the drift velocities of ions in noble gases as a function of E/p indicate that the ionic mobility varies with E/p as[11]

$$\mu^+(E/p)=\mu_0[1+\alpha_0(T/300)(E/p)]^{-1/2}. \tag{20}$$

Here μ_0 and α_0 are experimentally determined constants which are different for each gas. μ_0 is the "zero-field" mobility at 1 Torr and 300°K, while α_0 is the "high-field" mobility parameter. Δz_{drift} is then given by

$$\Delta z_{\text{drift}}=\mu^+[E_z(t_k)/p]E_z(t_k)\Delta t^+. \tag{21}$$

Here $E_z(t_k)$ is the z component of the electric field at the position of the ion at time t_k. A similar expression is used for Δr_{drift}.

The proposed model of ion diffusion is based upon the random walk model of Chandrasekhar.[12] In this approach, an expression is derived for the spatial and temporal distribution of a cloud of ions which are released from a point source and allowed to diffuse. From this, the cumulative probability that an ion will diffuse a distance Δx in a time Δt^+ may be derived. An isotropic angular distribution is also assumed. Then, by applying random number tests to the cumulative distribution functions, a distance and direction may be assigned to the diffusion of each ion during Δt^+, and the ion's coordinates may be shifted correspondingly. For diffusion in a two-dimensional Cartesian system (y, z) this leads to

$$\Delta y_{\text{diff}}=(-4D^+\Delta t^+\ln R_r)^{1/2}\sin 2\pi R_\psi \tag{22}$$

and

$$\Delta z_{\text{diff}}=(-4D^+\Delta t^+\ln R_r)^{1/2}\cos 2\pi R_\psi. \tag{23}$$

Here $D^+=(kT/e)\mu_0$, while R_r and R_ψ are random numbers uniformly distributed on the interval $[0, 1]$. The analogous equations in cylindrical coordinates are considerably more complicated.

Finally, if ions are to be updated, the ion distribution must be discretized, so that in the computation of charge density in Eq. (11), the replacement $n_{i,j}^+=B_n^+N_{i,j}^+$ is made with B_n^+ and $N_{i,j}^+$ defined similarly to B_n^- and $N_{i,j}^-$, respectively. Also, new ions must be created in the proper spatial and temporal distribution to replace those eliminated in crossing the boundaries. A possible method for doing this is presented in Ref. (1). The tracking of large numbers of particles of two species will, of course, require the use of a very fast digital computer with a large storage capacity.

[11] L. S. Frost, Phys. Rev. **105**, 354 (1957).

[12] S. Chandrasekhar, Rev. Mod. Phys. **15**, 1 (1943).